**Matthew L. Bauer**
Department of Mechanical and Aerospace Engineering,
University of Virginia,
Charlottesville, VA 22904-4746

**Christopher B. Saltonstall**
Department of Mechanical and Aerospace Engineering,
University of Virginia,
Charlottesville, VA 22904-4746

**Zayd C. Leseman**
Department of Mechanical and Industrial Engineering,
University of New Mexico,
Albuquerque, NM 87131

**Thomas E. Beechem**
Sandia National Laboratories,
Albuquerque, NM 87185

**Patrick E. Hopkins**
Department of Mechanical and Aerospace Engineering,
University of Virginia,
Charlottesville, VA 22904-4746

**Pamela M. Norris**
Department of Mechanical and Aerospace Engineering,
University of Virginia,
Charlottesville, VA 22904-4746

# Thermal Conductivity of Turbostratic Carbon Nanofiber Networks

*Composite material systems composed of a matrix of nanomaterials can achieve combinations of mechanical and thermophysical properties outside the range of traditional systems. The microstructure of the system dictates the rate, in which heat moves through the material. In this work, air/carbon nanofiber networks are studied to elucidate the system parameters influencing thermal transport. Thermal properties are measured with varying initial carbon fiber fill fraction, environment pressure, loading pressure, and heat treatment temperature (HTT) through a bidirectional modification of the 3ω technique. The nanostructure of the individual fibers is characterized with small angle X-ray scattering and Raman spectroscopy providing insight to individual fiber thermal conductivity. Measured thermal conductivity of the carbon nanofiber networks varied from 0.010 W/(m K) to 0.070 W/(m K). An understanding of the intrinsic properties of the individual fibers and the interactions of the two-phase composite is used to reconcile low measured thermal conductivities with predictive modeling. Accounting for fiber-to-fiber interactions and the nuanced changes in the composite as pressure is applied is necessary to successfully model thermal transport in system.* [DOI: 10.1115/1.4032610]

*Keywords: heat transfer, carbon fibers, 3ω technique, thermal conductivity, specific heat capacity, Raman spectroscopy, phonon mean free path*

## 1 Introduction

Carbon fibers and nanofibers have received much interest for simultaneously being strong, lightweight, and elastic with tunable thermal properties. This controllable thermal conductivity is ideal for optimizing properties to a specific application. Depending on the fabrication method and heat treatment process, the intrinsic thermal conductivity can span over several orders of magnitude [1]. The thermal conductivity of an individual fiber is strongly correlated to phonon mean free path (MFP), which is a function of the crystallite diameter. The size of the crystalline grains within the fiber can be tuned through heat treatment [2–4]. In the graphitic limit, an individual carbon fiber behaves much like a carbon nanotube (CNT) or graphene, with room temperature thermal conductivities as high as 1400 W/(m K) [5]. Conversely, in the turbostratic limit, in which small grain sizes limit phonon transport, thermal conductivity of the individual fibers approaches that of cross plane graphene, with reported values less than 20 W/(m K) [4]. Growth conditions dictate structural parameters and therefore thermal transport properties.

Thermal management applications utilizing carbon nanofibers require a composite material containing a matrix of fibers with an epoxy or a fluid filling the voids [6]. Such a composite can be tuned to meet the thermal and mechanical requirements of the application. However, it becomes more difficult to anticipate the total thermal transport as the system increases in complexity. The system geometry, interaction between materials, and deviation of each material from bulk, monolithic thermal properties influence the effective thermal conductivity of the system. Each of these terms must be accounted for to confidently predict how such a system will respond in a thermal management application. In the carbon fiber networks studied, these parameters are systematically varied to isolate the factors contributing the effective thermal transport of the system. To gain general insight into the mechanisms dictating the composite material's rate of heat flux, a series of thermal conductivity tests are performed with initial fiber fill fraction, HTT, loading pressure, and gas pressure varied. By observing the effects of fiber crystal size, fiber network density, particle orientation, fluid conductivity, and conductance via fiber-to-fiber contacts on the measured thermal conductivity, a link can be formed between the structural characteristics of the system and the resulting thermophysical properties. By generally considering the interdependent contributions of these features to thermal transport under the varied set of testing conditions, assurance is given for applying predictive thermal modeling to a broader range of fiber composite materials (varying the fluid material, type of fiber, fiber density, etc.) and the conditions in which they operate (such as straining the system). Furthermore, key considerations when designing fibrous thermal management solutions can be isolated.

## 2 Sample Preparation

The carbon nanofiber networks used in this work were synthesized using a chemical vapor deposition process. Palladium catalyst nanoparticles are initially heated in a furnace with an inert gas environment. Upon reaching 550 °C, an ethylene and oxygen

Contributed by the Heat Transfer Division of ASME for publication in the Journal of Heat Transfer. Manuscript received April 8, 2015; final manuscript received November 27, 2015; published online March 15, 2016. Assoc. Editor: Alan McGaughey.

mixture is passed over the Pd nanoparticles. Varying gas flow time alters the densities of the synthesized samples [7]. This fabrication method has been shown to create fibers with little atomic order [8].

Five unique samples were fabricated, labeled S1, S2, S3, S4, and S5 with respective densities of 90, 110, 130, 160, and 200 kg/m$^3$. Density measurements were taken with a vernier caliper and a precision weighing balance. Measurement error is estimated to be $\pm$ 10 kg/m$^3$. The samples have a cross-sectional area of approximately 10 mm $\times$ 10 mm and a height of 8 mm with fill fraction uniformity throughout the sample. By assuming an individual fiber density of 1700 kg/m$^3$ as has been measured on similar fibers [4], we infer an as-grown fill fraction, $\phi_0$, ranging from 5% to 12%. This term is not to be confused with the fill fraction of the samples under loading pressure, denoted by $\phi$. The least dense sample, S1, was divided into five parts. Four of these portions were heat treated at maximum HTT of 900 °C, 1100 °C, 1300 °C, and 1500 °C, respectively. The last portion underwent no heat treatment. Each heat treatment process took place in an inert argon environment with zirconium foil used as a getter to capture any remaining oxygen in the system. The temperature of the apparatus was ramped at a rate of 120 °C/hr until reaching the prescribed temperature. The samples were held at the respective maximum HTT for 2 hrs before cooling at the same rate they were heated. Each density measurement after heat treatment varied by no more than 5 kg/m$^3$ from the original measurement. This is within the measurement uncertainty, so we infer that the composite underwent no significant density change.

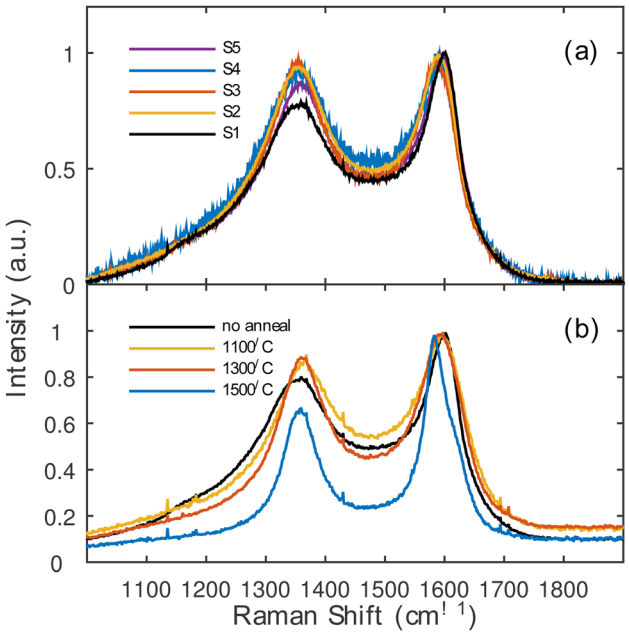


**Fig. 1 Average Raman spectra of each sample. Each spectrum was first normalized to the G peak intensity and then averaged. (*a*) The averaged spectra of the unannealed samples. (*b*) The averaged spectra of the annealed S1 series.**

## 3 Fiber Characterization

Prior to investigating the thermal transport in the carbon fiber network, it is necessary to understand the nature of the individual carbon fibers within the composite. The atomic structure of the carbon fibers dictates their intrinsic thermal conductivity, $k_f$, which influences the effective thermal conductivity of the system, $k_e$. The density of crystal boundaries as well as the size and density of voids within the fibers will determine the frequency at which thermal energy carriers scatter. A material's thermal conductivity is a function of the thermal energy carrier's scattering rate. Transmission electron microscopy (TEM) and Raman scattering are utilized to determine the size of the crystal boundaries to assess the scattering rate within the individual fibers.

TEM of similar carbon fibers shows a "herringbone" structure indicating that the fibers are made up of nanocrystalline graphite rather than amorphous carbon [8]. Nanocrystalline graphite is primarily composed of clusters of $sp^2$ bonded carbon, which are separated by grain boundaries and small regions of disorder. As thermal energy carriers travel through the nanocrystalline graphite, they scatter at each of these boundaries creating a resistance to thermal transport. Following the methodology of Ferrari and Robertson to implement the Tuinstra–Koenig relationship, Raman spectroscopy can be used to estimate the average diameter of these planar clusters through the relative intensities of the D peak ($\sim$1350 cm$^{-1}$) and the G peak ($\sim$1600 cm$^{-1}$) [9,10].

Raman spectra were collected using a Renishaw InVia Raman microscope. The system utilizes the 488 nm line of an Ar ion laser in 180 deg back scattering geometry and a 3000 g/mm grating. The sample was irradiated with 0.1 mW laser power through a 50 $\times$ 0.75 NA objective yielding a spot diameter of 900 nm. Ten spectra were collected, 360 s acquisition times, on each sample at ten different locations of the sample spaced 10 $\mu$m apart.

The average Raman spectra of the unannealed samples are plotted in Fig. 1(*a*). Each of the spectra is very similar indicating very little difference in the nanostructure from one sample to another. The calculated cluster diameter of the unannealed samples ranged from 41 $\pm$ 6 to 49 $\pm$ 5 Å confirming qualitative similarities. Since the cluster diameters are to first-order constant, the intrinsic thermal conductivity of the fibers is assumed constant as well. The changes in the effective thermal conductivity of the system must, therefore, arise from a source beyond that of the fibers themselves.

The impact of nanofiber ordering on the effective thermal conductivity was further investigated by examining samples annealed at temperatures ranging from 900 to 1500 °C. As shown in Fig. 1(*b*), the average Raman spectrum shows very little change upon annealing when exposed to temperatures less than 1500 °C. Quantitatively, employment of the Tuinstra–Koenig relationship provides a cluster diameter for samples annealed at 1100 and 1300 °C of 48 and 44 nm, respectively. These are within the range of that measured for the unannealed condition. Differences are found, however, upon annealing at 1500 °C where the average cluster diameter increases to 64 $\pm$ 32 nm. Although more nonuniform than those annealed at lower temperatures, the increase in cluster diameter for the high temperature anneal indicates an overall increase in crystal order. Better ordering, in turn, results in higher thermal conductivity. The results presented subsequently substantiate this line of thought where the high temperature anneal leads to an overall increase in thermal conductivity.

Small angle X-ray scattering (SAXS) data were acquired using Anton Paar's SAXSESS MC$^2$ tool operating at 40 kV and 30 mA with the incident beam line collimated. Data were collected on imaging plates and desmeared prior to analysis. X-ray scattering experiments measure the angle, $\theta$, and intensity, $I$, with which incident radiation scatters from a sample. The exit angle is considered in terms of the wave form vector: $q = 4\pi/\lambda \sin(\theta)$ with the X-ray wavelength $\lambda = 1.5418$ Å. This diffuse scattering is caused by spatial fluctuations in electron density, allowing it to be used to characterize the nanostructure of multiphase systems. The scattered X-rays' exit angle corresponds to features of regularly occurring particles. Larger particle features influence the data at smaller angles. Ideally, SAXS experiments complement microscopy experiments by identifying a statistically significant average of the feature of interest.

In the case of carbon fibers, previous works have demonstrated an ability to characterize the dimensions of the voids contained within the individual fibers [11–13]. These studies looked at systems with long crystalline regions, creating the opportunity for

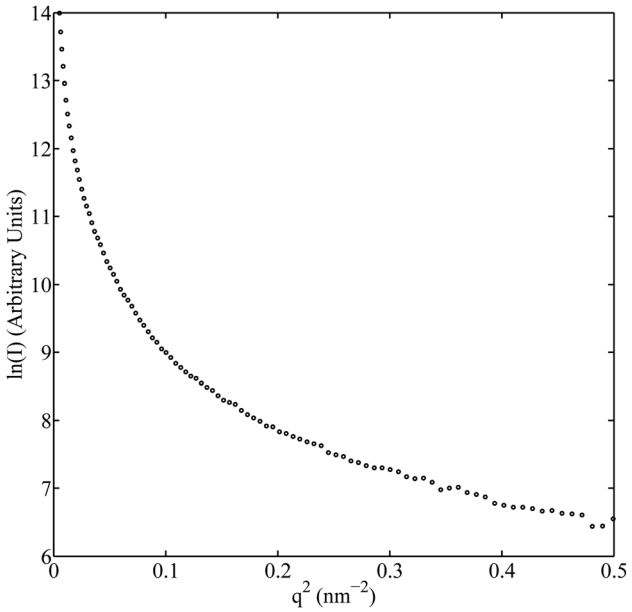


**Fig. 2 Guinier plot of SAXS intensity decay. The lack of linear region over this *q* regime indicates an absence of monodisperse voids observed in other carbon fiber samples.**

strain to pull the planes of carbon apart. In the same manner, we generate a Guinier plot of our data in the low angle regime in Fig. 2. From the slope and intercept of such a plot, it is possible to determine the radius of gyration and cross-sectional area of an included particle (or void) of appropriate size in the system due to variations in the electron density between the included particle and host material. However, the lack of a linear region in our data indicates voids similar to those observed by other authors that do not exist. TEM of similar turbostratic samples helps to confirm this result [8]. Data taken on each fabricated sample displayed nearly identical trends to that shown in Fig. 2. We conclude that voids with diameters on the order of a few nanometers do not exist in these samples. This result simplifies thermal modeling considerations as the presence of voids would alter the scattering rate of thermal energy carriers.

Scanning electron microscope images of the samples are shown in Fig. 3. Each sample displays the highly entangled nature of the fiber composites, a relatively low fill fraction, and the regularity of fiber-to-fiber contacts. From these images, we infer a fiber diameter on the order of 100 nm. This value is used to estimate pore size [14] and therefore gas thermal conductivity, $k_g$. Additionally, rod diameter influences the Hertzian contact radius which varies fiber-to-fiber contact conductance as pressure is applied as explained in Sec. 4. These images give confidence to the assumption of random fiber orientation used to model the network.

## 4 Thermal Characterization and Modeling

The $3\omega$ technique was utilized to characterize the thermal conductivity and volumetric heat capacity of the samples. The concept of a bidirectional $3\omega$ technique as well as our experimental details is discussed elsewhere [15–17]. This methodology is necessary due to the difficulty of depositing the requisite linear thin metal wire directly onto the system and impossibility of maintaining constant wire dimensions of this metal line as pressure is applied and the sample is compressed. The heating wire is deposited on an insulative polymer layer (hard baked SU-8 3025) with $SiO_x$ passivation layer 240 nm thick deposited onto the wire. An ac signal passing through the wire induces the measurable third harmonic voltage drop across the heating line, $V_{3\omega}$, which can be related to the ac temperature rise, $T_{2\omega}$, by first determining the thermoresistive response of the wire. The properties of the heating line and $T_{2\omega}$ are used to solve the heat diffusion equation for the sample for a given driving frequency.

The thermal conductivity of the $SiO_x$ layer is independently measured to have a thermal conductivity of 0.91 W/(m K). The previous studies have measured $SiO_2$ thin films slightly below 1 W/(m K) near 200 nm thickness [18]. The heating line is used to test the thermal conductivity of the polymer layer under vacuum similar to traditional $3\omega$ experiments [19]. This yields a thermal conductivity of 0.14 W/(m K), which is similar to the advertised thermal conductivity from the manufacturer, MicroChem, of 0.2 W/(m K) as well as that measured by others [20]. With these inputs known, the thermal properties of the carbon fiber networks can be characterized with three fitting parameters: the samples' effective thermal conductivity and volumetric heat capacity as well as the contact resistance between the passivation layer and the sample ($k_e$, $C_e$, and $R_p$, respectively). Each sample is pressed onto the passivation layer directly above the heating line with a plate on the backside of the sample. Pressure is applied by tightening screws connecting this plate to the sample mount. The properties of the screws and the torque required to tighten each screw are used to approximate the pressure applied to the sample. Heat travels from the metal wire into both the polymer layer as well as the sample. Frequency sweeps from 1 to 10,000 Hz allow the simultaneous fitting of each parameter. Data were analyzed accounting for bidirectional heat flow from the heating wire [15,19,21]. Due to the length scale of the samples tested and the small temperature rise necessary for $3\omega$ experiments, the effects of blackbody radiation can be approximated as less than 2% [22]. Example raw data are plotted in Fig. 4.

Figure 5 demonstrates the unique sensitivity to each parameter for the frequency range tested, indicating that the three parameters can be fit simultaneously. Here, the sensitivity parameter is defined as

$$S_p = \frac{\left(V_{3\omega}(\Delta) - V_{3\omega}(0)\right)/V_{3\omega}(0)}{(\Delta p - p)/p} = \frac{V_{3\omega}(\Delta) - V_{3\omega}(0)}{V_{3\omega}\Delta} \quad (1)$$

in which the parameter of interest $p$ is perturbed by amount $\Delta$ for which we select 10%. As can be seen, each fitting parameter

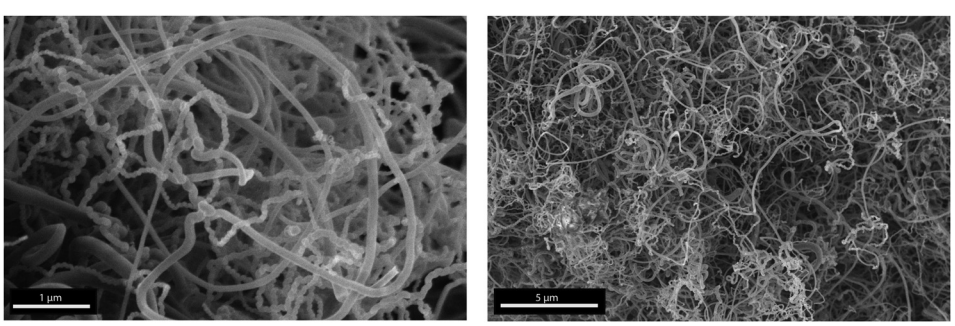


**Fig. 3 Scanning electron microscope image of a carbon fiber sample**

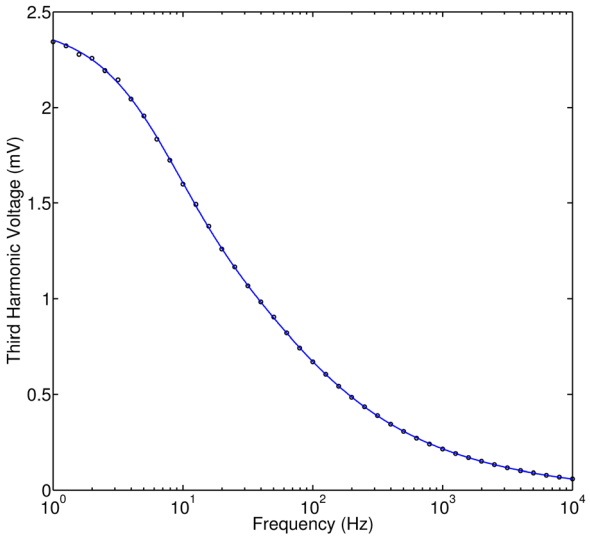


**Fig. 4 Raw data and modeled fit from sample S1 with an applied pressure of 220 kPa. The experimental uncertainty in each data point is slightly smaller than the data markers. The measured values match the inputs used in Fig. 5.**

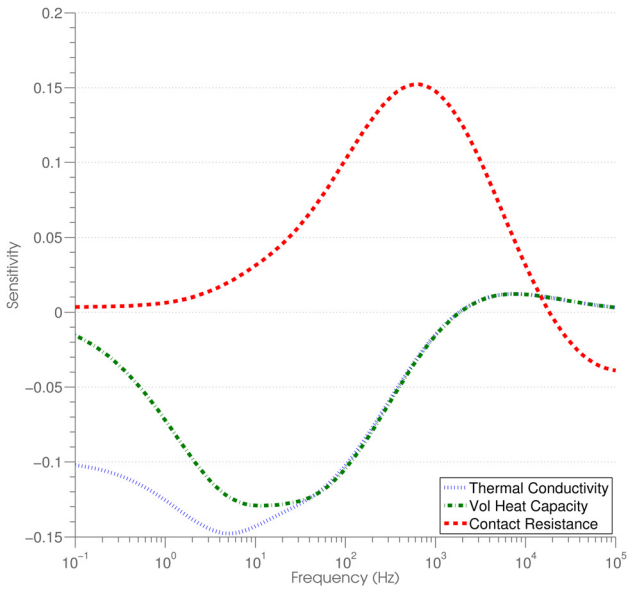


**Fig. 5 Sensitivity of the 3$\omega$ experiment to composite samples' effective thermal conductivity and volumetric heat capacity as well as the contact resistance between the mount and sample. This plot was generated with $k_e = 0.024$ W/(m K), $C_e = 3 \times 10^5$ J/(m$^3$ K), and $R_p = 6 \times 10^{-5}$ K m$^2$/W, similar to the fourth data point in Fig. 6. The change in direction of the contact resistance sensitivity above 10,000 Hz only exists due to the presence of the $SiO_x$ layer closer to the heater. At greater applied pressures, the signal's sensitivity to the carbon fibers' thermal conductivity and heat capacity is increased. At low applied pressures, the experiment can lose sensitivity to these properties [15].**

exhibits a unique sensitivity trend. Both $k_e$ and $C_e$ become uniquely identifiable below 100 Hz and particularly below 10 Hz at which point the contact resistance sensitivity effects become minimal. At lower frequencies, the measured third harmonic waves are sensitive to properties deeper into the sample, making the relative contribution of the contact resistance negligible. However at higher frequencies, thermophysical properties closer to the heating wire dominate the signal, causing greater sensitivity to the contact resistance and properties of the passivation layer. The

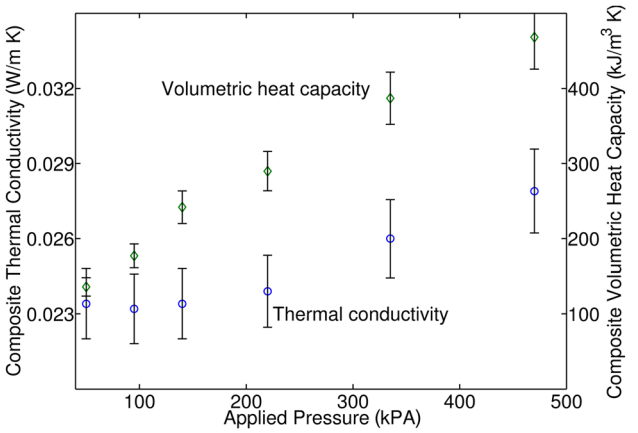


**Fig. 6 Best fit results of data taken on S1 (without heat treatment) with measured density of 90 kg/m$^3$. Measurements were taken at six unique compressive pressures, with the sample thermal conductivity, sample volumetric heat capacity, and the sample to mount contact resistance simultaneously fit. This data are representative of data taken on each sample. The fitting error propagated from sources of uncertainty in the system is estimated at 9% for the sample's thermal conductivity, 6% for the volumetric heat capacity, and 4% for the contact resistance between the sample and the passivation layer.**

experiment was repeated on each sample with the loading pressure systematically varied. As the axial loading pressure is increased, the density of the sample increases, altering the properties of the sample and the contact resistance. The discussion of this particular technique and demonstrations of data fitting for samples with similar values to those studied in this work can be found in the previous work [15].

Figure 6 displays the fitted results for data taken at atmospheric pressure on the portion of S1 which did not undergo heat treatment. The volumetric heat capacity, $C_e$, varies linearly with pressure. This trend can be attributed to a change in density of the composite when the macroporous voids shrink as the sample is compressed. The linear nature of this trend at low loading pressures confirms this conclusion. We assume that the heat capacity per unit mass of the nonwoven carbon nanofibers, $c_m$, is approximately 710 J/kg K. With this information, we can approximate the fill fraction of the sample during each measurement

$$\phi = C_e/(c_m \rho_0) \tag{2}$$

A loading pressure ranging from 50 to 470 kPa caused the density of the 90 kg/m$^3$ sample (implying a $\phi_0 = 5\%$ fill fraction) to vary from 10% to over 40% fill fraction. Over this pressure range, the best fit contact resistance varied from $10^{-4}$ to $5 \times 10^{-5}$ m$^2$K/W. Also indicated in Fig. 6 is the gradual increasing trend of the effective sample thermal conductivity as greater pressure is applied. This result is representative for all the samples which did not undergo heat treatment. Using Eq. (2) and the measured volumetric heat capacity, the carbon fiber fill fraction is able to be inferred at each pressure. This changing fill fraction can be used to approximate structural parameters which change as pressure is applied. Knowledge of these parameters (such as pore size, fiber orientation, fiber contact density, etc.) is subsequently used to understand the measured thermal conductivity values on each sample in each scenario. The measured thermal conductivity values ranging from 0.023 W/m K to 0.028 W/m K is similar to measurements made on randomly aligned CNTs of much lower densities [23] and much lower than CNT samples of comparable densities [24].

To understand the best fit thermal conductivity values, the properties of the carbon fibers, fiber-to-fiber interactions, and the air host are considered. Previous work has measured the thermal conductivity of individual carbon fibers with short coherence

length [4]. Qiu et al. provided a linear fit of thermal conductivity versus coherence length which leads to an approximation of the intrinsic thermal conductivity of the individual fibers. The nonheat-treated samples tested in this work have an estimated intrinsic fiber conductivity near 40 W/m K based on this linear approximation and the cluster diameter determined from the Raman measurements.

For fibrous insulation type materials of similar densities and length scales, Bhattacharyya demonstrated that the contribution of convection is negligible [25]. Conduction through the air phase is a function of temperature, the pressure of the atmosphere, and the air molecules' MFP between scattering events, $\lambda$. For air in an infinitely large medium, the bulk MFP ($\lambda_B$) is 68 nm at standard temperature and pressure, which results in the thermal conductivity of air of 0.026 W/m K [26]. The structurally limited MFP of air in entangled fibrous networks can be approximated [14] as $\lambda_n = \pi r/2\phi$, where $r$ is the fiber radius which is approximated as 50 nm from the SEM images. As the Knudsen number increases ($\mathrm{Kn} = \lambda_B/\lambda_N$), the thermal conductivity of the gas decreases. Furthermore, in a porous solid with a Knudsen number greater than 0.01, the gas cannot be assumed to be in the continuum regime. Gas conduction will begin to transit to the free molecule regime [27]. Therefore, the thermal accommodation coefficient (TAC), which relates the efficiency of energy transfer between a surface and gas, must also be considered to predict the thermal transport within the gas [28]. This has been shown to influence gas behavior in similar porous carbon materials [23]. Accurately identifying a TAC over a wide range of scenarios is an ongoing area of research. Relating robust predictive transport models with measured results of open fiber systems can be limited by a lack of experimental data for TAC [27].

Previous work has demonstrated strongly influential TAC in small diameter CNT aerogels. Furthermore, the TAC is diameter dependent in CNT systems. Research has shown that as CNT diameters increased to 6 nm, the simulated TAC became similar to graphene [29]. However, factors like fiber roughness can further alter the ratio of thermal energy absorbed to thermal energy reflected even in otherwise similar carbon systems. This effect may cause carbon fibers to not be directly comparable to CNTs. Additionally, experimental comparison is limited by the corresponding gaseous environment. The research has suggested that the TAC in argon is similar to (but slightly greater than) $N_2$ or air environments [30,31]. Carbon materials in argon environments have been shown to have a TAC on the order of 0.9 [29,28]. Schiffres et al. demonstrated that accounting for TAC by calculating the energy limited MFP a gas will travel and using Matthiessen's rule to incorporate this value into gas thermal conductivity kinetic theory [23]. Lower TAC causes longer thermal memory within the gas molecules. By using an approximation for TAC of 0.9, the gas thermal conductivity values in this work would increase by 6–9%.

However, an exact accommodation coefficient is not known for all the material combinations. With this in mind, an accommodation coefficient of 1 was used to generate thermal models in this work. We note that selecting a lower TAC decreases the discrepancy between the model and experimental data shown later in Fig. 7. With this simplification, the thermal conductivity of the gas phase ($k_g$) of our samples at the smallest applied axial load pressure is approximated as 0.009 W/m K. This value decreases with added pressure. At the greatest applied pressure, $k_g$ is approximately 0.005 W/m K due to a decrease in pore size which increases the scattering rate of the air molecules. In the case of S5 tested at vacuum pressure of 0.1 Pa, the thermal conductivity of the gas phase at these reduced dimensions is negligible [32].

Calculating the composite's effective thermal conductivity, $k_e$, using a simple rule of mixing as the weighted average of the two phases, $k_e = \phi k_f + (1-\phi)k_g$, overpredicts our results by 2 orders of magnitude. To gain insight into the origins of this reduction of thermal conductivity, we consider the microstructure of the sample. Fricke's method for predicting electrical conductivity of disperse suspensions [33] can be used to predict the thermal conductivity of rods if the sample can be assumed as a homogenous medium with fiber interaction averaged over the unit cell volume [25]. By defining the ratio of thermal conductivity, $C_r = k_g/k_f$, and the volume ratio $V_r = \rho/(\rho_0 - \rho)$, Bhattacharyya used Fricke's method to predict the thermal conductivity of a composite with fibers perpendicular to heat flow as [25]

$$k^B = k_f\left(1 - \frac{1 - C_r}{1 + (2C_rV_r)/(1 + C_r)}\right) \tag{3}$$

This model predicts the correct order of magnitude compared to the measurements in this work but fails to capture the trend as pressure is applied. Stark and Fricke build upon Bhattacharyya's model by first modifying the equation for the representative unit cell to be a function of average fiber orientation, $Z$ [34]

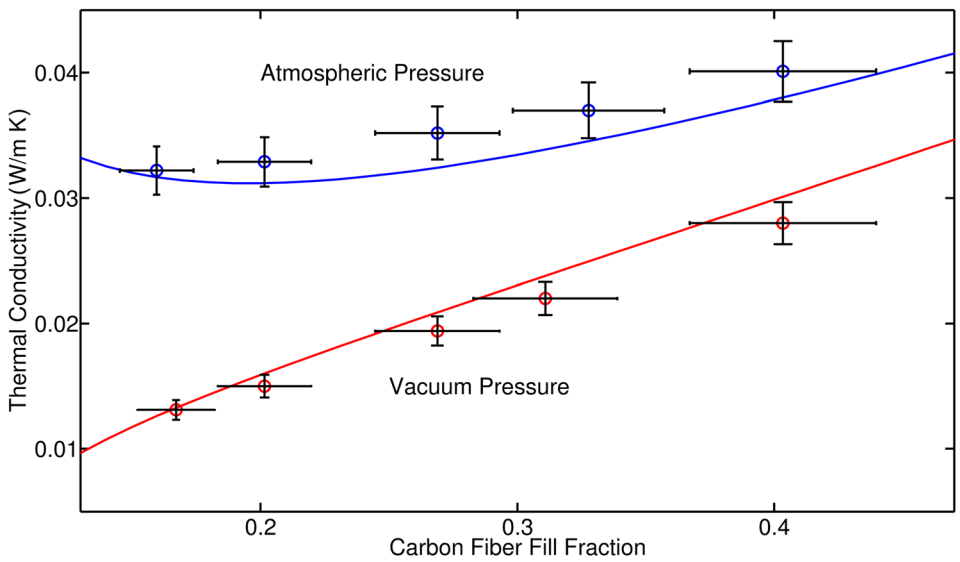


**Fig. 7 Measured thermal conductivity values from sample S5 at both vacuum and atmospheric pressure. Carbon fill fraction is calculated from the best fit volumetric heat capacity using Eq. (2). Also, plotted is the SFM accounting for varying sample properties as pressure is applied.**

$$k^{BZ} = k_f\left(1 + \frac{C_r + 1}{1 + V_r\left(1 + Z(C_r - 1)/(C_r + 1)\right)}\right) \tag{4}$$

Stark and Fricke then advance the model by taking into account the fiber-to-fiber interactions as part of a resistor network. The effective thermal resistance from fiber-to-fiber contacts in a unit cell is [34]

$$R_{ct} = \frac{j\pi a_{ct}}{4k_f A r} \tag{5}$$

where $r$ is the fiber radius, $A$ is a connection parameter equal to 0.611, $j$ is a parameter defining the unit cell area, and $a_{ct}$ is the radius of the contact between the fibers. We estimate the resistance due to an individual fiber-to-fiber contact to be on the order of $10^5$ K/W. For reference, others studying CNT contact resistances without an external applied compressive force and with rod diameter, an order of magnitude is smaller to find contact resistances on the order of $10^7$ K/W [35,36]. By incorporating $R_{ct}$ and $k^{BZ}$ into a resistor network and leaving $Z$ as a fitting parameter, Stark and Fricke succeeded in matching their thermal model to a large variety of thermal conductivity data for insulation type materials with $Z$ varying from 0.66 to 0.97.

To accurately apply the Stark and Fricke model (SFM) to describe the thermal transport in each sample, we must take into account the parameters that vary as pressure is applied: $Z$, $\phi$, $k_g$, and $R_{ct}$. As previously stated, we determine fiber fill fraction, $\phi$, from the best fit volumetric heat capacity, and gas conductivity, $k_g$, is approximated from the previously developed models [27]. For any fibrous composite, the average fiber orientation is difficult to independently measure. When all the rods are perpendicular or parallel to the flow of heat, $Z = 1$ or $Z = 0$, respectively, while $Z = 2/3$ indicates completely random orientation in three-dimensional space. To avoid attempting to overfit the data, we assume that the average fiber is completely randomly oriented, and $Z = 2/3$ is used in all the scenarios prior to pressure being applied to the sample. We then assume that as we apply pressure to our samples, the increased density incorporates new perpendicular rods while removing rods parallel to heat flow, i.e., bending rods over. Therefore, we can calculate the increase in $Z$ at each successive pressure as a function of the changing density of the sample, as determined from the fit volumetric specific heat. Let the ratio of perpendicular to parallel rods at any pressure be $R_Z(n)$ and $Z(0)$ be the orientation when no pressure is applied. Then, at each increased density, the ratio can be calculated and used to determine the new average fiber orientation

$$R_Z(n) = \frac{\phi(0)Z(0) + \phi(n) - \phi(0)}{(1 - Z(0))\phi(0)} \tag{6}$$

$$Z(n) = R_Z(n)/(R_Z(n) + 1) \tag{7}$$

Finally, the path of thermal conductance between fiber contacts varies as pressure is applied: the size of the representative unit cell is altered (and the cell density), the contact area between the fibers varies, and the individual fiber-to-fiber contact resistance also varies as a function of pressure. For a bed of fibers, the Hertzian contact radius can be calculated [14]

$$a_{ct} = \left(\frac{3}{2}\frac{(1 - \mu^2)}{E}P_1 r\right)^{1/3} \tag{8}$$

in which $\mu$ is the Poisson's ratio, $E$ is the Young's modulus, and $P_1$, the load on an individual contact, is a function of the applied pressure, $p$

$$P_1 = p\left(\frac{\pi r}{2\phi Z}\right)^2 \tag{9}$$

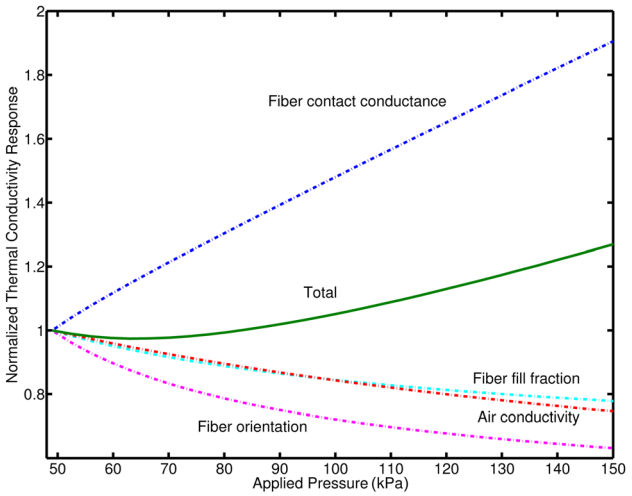


**Fig. 8 Normalized modeled response of 200 kg/m$^3$ dense carbon nanofiber composite (S5) as pressure is applied. The total thermal conductivity response, $k_e$, only increases due to the role of thermal conductance through fiber contacts. Alternatively, increasing carbon fiber fill fraction does not increase effective thermal transport while excluding additional fiber-to-fiber contacts. The contribution of gas conductivity decreases at greater pressures due to decreasing pore sizes. The bending over of fibers at greater applied pressures also causes a decrease in the thermal conductivity.**

Knowing the applied pressure and contact radius, Eq. (5) can be used to determine the effective contact resistance through the fiber-to-fiber contacts. With $R_{ct}$, $Z$, $\phi$, $k_f$, and $k_g$ determined, the SFM can be used to calculate the thermal conductivity and the results can be compared directly to the measured $3\omega$ results without fitting parameters.

Figure 8 demonstrates the isolated effects of fiber orientation, density, air conductivity, and the contact resistance term on the modeled thermal conductivity (each term that varies as pressure is applied) for a sample with an initial density of 200 kg/m$^3$, where $k_f = 40$ W/(m K) has been assumed. The positive effective thermal conductivity trend when pressure is applied can only be a result of the interactions between touching fibers. Other models which predict the effective thermal conductivity of two-phase media that do not take into account the interactions of the included particles, such as effective medium theory, cannot replicate this trend. In other scenarios in which the sample has different properties, such as assuming an increased intrinsic fiber conductivity, or higher percentage of fibers parallel to heat flow, the response of $k_e$ to fiber fill fraction, $\phi$, is positive when pressure is applied.

Figure 7 displays the best fit sample thermal conductivity, $k_e$, of S5 at atmospheric pressure and under vacuum plotted against the calculated carbon fiber fill fraction, $\phi$, as determined from the best fit volumetric specific heat of the sample. The results of the SFM are also plotted in Fig. 7 with the appropriate inputs recalculated at each pressure. When no pressure is applied, $\phi = 12\%$. As highlighted in Fig. 8, the increase in thermal conductivity as pressure is applied is a result of the increase in the conductance path between interacting fibers. The relative shift between thermal conductivity at atmospheric pressure and vacuum pressure decreases at higher fill fraction. At atmospheric pressure, shrinking pore size decreases the MFP of air molecules (increasing the Knudsen number) ultimately causing conduction through the gas to contribute a smaller portion to the sample's effective thermal conductivity. In the data series taken at vacuum pressure, $k_g$ is negligible at each data point. In the limit, as the MFP of the air approaches zero due to infinitely small pores, the thermal conductivity of the samples measured at atmospheric conditions would approach the same value as the measured result with the sample held under vacuum.

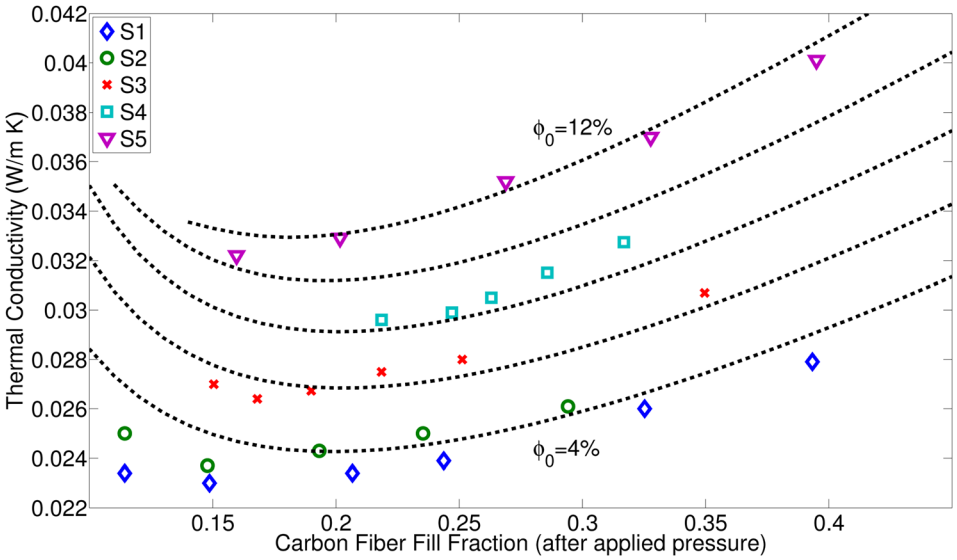


**Fig. 9 Best fit 3$\omega$ thermal conductivity results for nonheat-treated samples S1, S2, S3, S4, and S5 (densities of 90, 110, 130, 160, and 200 kg/m$^3$, respectively). All the data are acquired at room temperature and atmospheric pressure. The thermal conductivity predictions from the SFM (dashed lines) are also plotted for initial fill fractions ranging from 4% to 12% in steps of 2% ($\phi_0$). As pressure is applied, the fill fraction increases to a maximum value of $\phi = 40\%$.**

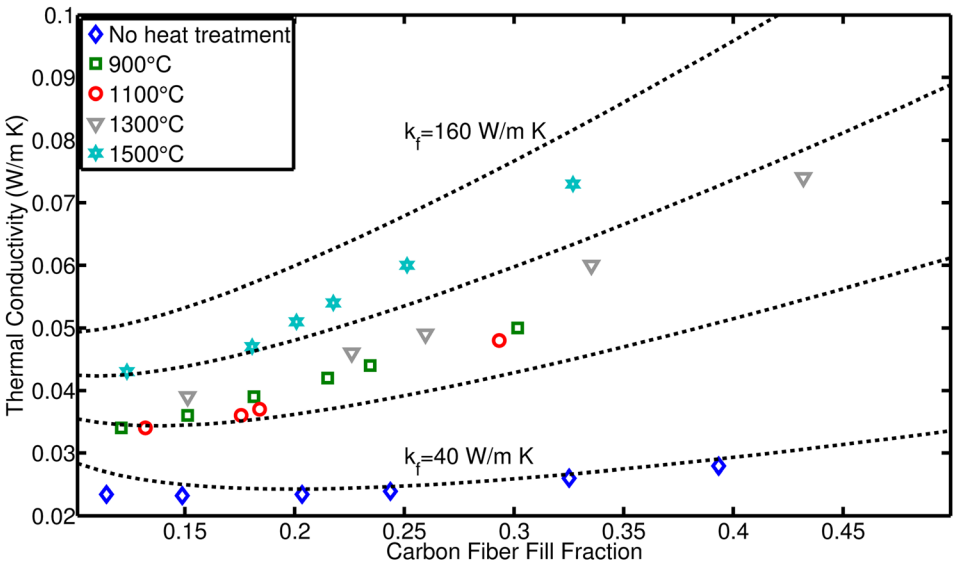


**Fig. 10 Best fit data from the heat-treated sample series (S1). The measured thermal conductivity increases significantly from the as-grown sample compared to the heat-treated samples, with the sample which underwent a 1500 °C HTT showing an additional increase compared to the more moderately heated samples. The change in effective thermal conductivity with respect to carbon fiber fill fraction has increased with heat treatment. Over the data, the SFM is plotted with carbon fiber thermal conductivities of 40, 80, 120, and 160 W/(m K), respectively.**

The measurements of samples having variable initial fill fraction further underscore the utility of the SFM as shown in the data of Fig. 9. Again, the SFM with the discussed parameter trends is plotted over the best fit results (dashed lines), however, the input initial fill fraction, $\phi_0$, value used for the model is systematically changed from 4% to 12% in increments of 2%. By accounting for each changing parameter, the SFM accurately predicts both the magnitude of $k_e$ and the trend as pressure is applied. Interestingly, the thermal conductivity of the samples with low initial density at high applied pressure (e.g., $S_1$ at $\phi = 40\%$ has $k_e = 0.027 \pm 0.0024$ W/m K) remains significantly less than samples with higher initial fill fraction when minimal pressure is applied (e.g., $S_5$ at $\phi = 16\%$ has $k_e = 0.032 \pm 0.0028$ W/m K). It is apparent that for material systems of similar intrinsic properties, the initial fill fraction of the system is more important than the resulting fill fraction if a compressive force is applied to the system while it is operating. Even though at increased applied pressures there is increasing conductance between touching rods, rods changing from near parallel to near perpendicular to the heat flux can nearly negate this contribution.

Finally, the role of intrinsic fiber thermal conductivity is examined using the dependence of thermal conductivity on the heat treatment as shown in Fig. 10. Similar to Fig. 9, the SFM is plotted over this data. Here, the input fiber thermal conductivity, $k_f$, is

systematically varied from 40 to 160 mW/m K to reflect the anticipated change resulting from the heat treatment process on the samples. As expected, heat treating results in a measurable increase in sample thermal conductivity, $k_e$, which is likely caused by increasing $k_f$. This result is most apparent at the HTT of 1500 °C in which we infer that $k_f$ has increased to around 120 mW/m K. This agrees with the Raman measurements indicating that crystalline MFP has increased compared to the as-grown samples. The three samples heat treated at maximum temperatures of 900 °C, 1100 °C, and 1300 °C showed a more moderate increase compared to the nonheat-treated sample, with an apparent fiber thermal conductivity around 80–100 mW/m K. The increased intrinsic fiber conductivity causes a more rapid rise in the effective sample thermal conductivity as pressure is applied. Over the relatively moderate pressure range tested, the 1500 °C HTT sample exhibited a 50% thermal conductivity increase while the nonheat-treated samples exhibited increases closer to 20%. Composites with high intrinsic conductivity fibers increase in conductivity more rapidly as pressure is applied.

## 5 Conclusions

Fiber networks are increasingly being utilized in microsystems requiring thermal management. Predicting thermal transport in composite systems requires an understanding of each phase as well as their interactions. The predictive models that do not take into account interactions between the individual fibers do a poor job of anticipating thermal transport in networks of fibers. Through thermal conductivity measurements under varying compressing pressures on composite carbon fiber networks, it is shown that the thermal pathway between touching fibers must be accounted for to predict increased thermal transport as greater pressure is applied. Beyond this, methods for accounting for other contributions to thermal transport in composites are highlighted including the role of the fluid within the composite's pores and fibers bending as pressure is applied. The strong influence of the initial fiber fill fraction is shown to be often more important for minimizing the thermal transport than the fill fraction after compression. Finally, the intrinsic fiber conductivity displays an increasingly strong influence on the composite's thermal conductivity at greater applied pressures for systems of similar initial fill fractions.


## Acknowledgment

The small angle X-ray scattering experimental work was conducted at the Center for Nanophase Materials Sciences, which was sponsored at the Oak Ridge National Laboratory by the Scientific User Facilities Division, Office of Basic Energy Sciences, U.S. Department of Energy. The authors appreciate the support from the National Science Foundation Grant No. CMMI-1229603. This work was partially supported by the Army Research Office, Grant No. W911NF-13-1-0378. The authors would also like to thank Professor Elizabeth Opila for the laboratory and equipments to use to heat treat the samples.


## Nomenclature

$a_{ct}$ = fiber contact radius (m)
$c_m$ = specific heat capacity (J/(kg K))
$C_e$ = volumetric heat capacity (J/(m$^3$ K))
$C_r$ = conductivity ratio
$k_e$ = effective composite thermal conductivity (W/(m K))
$k_f$ = individual carbon fiber thermal conductivity (W/(m K))
$k_g$ = gas thermal conductivity (W/(m K))
Kn = Knudsen number
$p$ = parameter of interest
$P_1$ = load between two fibers
$q$ = X-ray scattering vector (m$^{-1}$)
$r$ = fiber radius (m)
$R_p$ = sample to experiment thermal contact resistance (K m$^2$/W)
$R_Z$ = ratio of fibers perpendicular and parallel to heat flow
$R_{ct}$ = fiber-to-fiber thermal contact resistance (K m$^2$/W)
$S_p$ = experimental sensitivity to a given parameter
$V_r$ = volume ratio
$V_{3\omega}$ = third harmonic voltage (V)
$Z$ = normalized fiber orientation
$\theta$ = scattering angle
$\lambda$ = X-ray wavelength (m)
$\lambda$ = mean free path (m)
$\lambda_B$ = bulk mean free path (m)
$\lambda_N$ = structurally limited mean free path (m)
$\mu$ = Poisson's ratio
$\rho$ = sample density (kg/m$^3$)
$\rho_0$ = sample density, as grown (no pressure applied) (kg/m$^3$)
$\phi$ = sample fill fraction
$\phi_0$ = sample fill fraction, as grown (no pressure applied)

## References


[1] Peebles, L., Jr., 1995, *Carbon Fibers: Formation, Structure, and Properties*, CRC Press, Boca Raton, FL.
[2] Heremans, J., Rahim, I., and Dresselhaus, M. S., 1985, "Thermal Conductivity and Raman Spectra of Carbon Fibers," Phys. Rev. B, **32**(10), pp. 6742–6747.
[3] Mayhew, E., and Prakash, V., 2013, "Thermal Conductivity of Individual Carbon Nanofibers," Carbon, **62**, pp. 493–500.
[4] Qiu, L., Zheng, X., Zhu, J., Su, G., and Tang, D., 2013, "The Effect of Grain Size on the Lattice Thermal Conductivity of an Individual Polyacrylonitrile-Based Carbon Fiber," Carbon, **51**, pp. 265–273.
[5] Piraux, L., Nysten, B., Haquenne, A., Issi, J.-P., Dresselhaus, M., and Endo, M., 1984, "The Temperature Variation of the Thermal Conductivity of Benzene-Derived Carbon Fibers," Solid State Commun., **50**(8), pp. 697–700.
[6] Chung, D., 2001, "Materials for Thermal Conduction," Appl. Therm. Eng., **21**(16), pp. 1593–1605.
[7] Atwater, M. A., Mousavi, A. K., Leseman, Z. C., and Phillips, J., 2013, "Direct Synthesis and Characterization of a Nonwoven Structure Comprised of Carbon Nanofibers," Carbon, **57**, pp. 363–370.
[8] Atwater, M. A., Phillips, J., Doorn, S. K., Luhrs, C. C., Fernández, Y., Menéndez, J., and Leseman, Z. C., 2009, "The Production of Carbon Nanofibers and Thin Films on Palladium Catalysts From Ethylene–Oxygen Mixtures," Carbon, **47**(9), pp. 2269–2280.
[9] Tuinstra, F., and Koenig, J. L., 1970, "Raman Spectrum of Graphite," J. Chem. Phys., **53**(3), pp. 1126–1130.
[10] Ferrari, A. C., and Robertson, J., 2000, "Interpretation of Raman Spectra of Disordered and Amorphous Carbon," Phys. Rev. B, **61**(20), pp. 14095–14107.
[11] Fourdeux, A., Herinckx, C., Perret, R., and Ruland, W., 1970, "La structure des fibres de carbone," Compt. Rend. Acad. Sci., **25**(1969), pp. 1507–1600.
[12] Gupta, A., Harrison, I. R., and Lahijani, J., 1994, "Small-Angle X-Ray Scattering in Carbon Fibers," J. Appl. Crystallogr., **27**(4), pp. 627–636.
[13] Shioya, M., and Takaku, A., 1985, "Characterization of Microvoids in Carbon Fibers by Absolute Small-Angle X-Ray Measurements on a Fiber Bundle," J. Appl. Phys., **58**(11), pp. 4074–4082.
[14] Kaganer, M. G., 1969, *Thermal Insulation in Cryogenic Engineering*, Israel Program for Scientific Translations, Jerusalem, Israel.
[15] Bauer, M. L., and Norris, P. M., 2014, "General Bidirectional Thermal Characterization Via the 3$\omega$ Technique," Rev. Sci. Instrum., **85**(6), p. 064903.
[16] Hu, X., Padilla, A., Xu, J., Fisher, T., and Goodson, K., 2006, "3-Omega Measurements of Vertically Oriented Carbon Nanotubes on Silicon," ASME J. Heat Transfer, **128**(11), pp. 1109–1113.
[17] Qiu, L., Tang, D. W., Zheng, X. H., and Su, G. P., 2011, "The Freestanding Sensor-Based 3$\omega$ Technique for Measuring Thermal Conductivity of Solids: Principle and Examination," Rev. Sci. Instrum., **82**(4), p. 045106.
[18] Lee, S.-M., and Cahill, D., 1997, "Heat Transport in Thin Dielectric Films," J. Appl. Phys., **81**(6), pp. 2590–2595.
[19] Kim, J. H., Feldman, A., and Novotny, D., 1999, "Application of the Three Omega Thermal Conductivity Measurement Method to a Film on a Substrate of Finite Thickness," J. Appl. Phys., **86**(7), pp. 3959–3963.
[20] Sun, W.-C., Huang, M.-J., Chien, H.-C., Chang, T.-Y., and Yao, D.-J., 2010, "A Novel Method for Measuring Thick Film Thermal Conductivity," 5th IEEE International Conference on Nano/Micro-Engineered and Molecular Systems (NEMS), Xiamen, China, Jan. 20–23, pp. 1052–1056.
[21] Feldman, A., 1999, "Algorithm for Solutions of the Thermal Diffusion Equation in a Stratified Medium With a Modulated Heating Source," High Temp. High Pressures, **31**(3), pp. 293–298.
[22] Cahill, D., 1990, "Thermal Conductivity Measurement From 30 to 750 K: The 3$\omega$ Method," Rev. Sci. Instrum., **61**(2), pp. 802–808.
[23] Schiffres, S. N., Kim, K. H., Hu, L., McGaughey, A. J. H., Islam, M. F., and Malen, J. A., 2012, "Gas Diffusion, Energy Transport, and Thermal Accommodation in Single-Walled Carbon Nanotube Aerogels," Adv. Funct. Mater., **22**(24), pp. 5251–5258.

[24] Prasher, R. S., Hu, X. J., Chalopin, Y., Mingo, N., Lofgreen, K., Volz, S., Cleri, F., and Keblinski, P., 2009, "Turning Carbon Nanotubes From Exceptional Heat Conductors Into Insulators," Phys. Rev. Lett., **102**(10), p. 105901.
[25] Bhattacharyya, R. K., 1980, *Heat-Transfer Model for Fibrous Insulations, Thermal Insulation Performance*, American Society for Testing and Materials, Philadelphia, PA, pp. 272–286.
[26] General Electric Company, Research and Development Center, 1984, *Heat Transfer and Fluid Flow Data Books*, Genium Publishing, Schenectady NY.
[27] Raed, K., and Gross, U., 2009, "Modeling of Influence of Gas Atmosphere and Pore-Size Distribution on the Effective Thermal Conductivity of Knudsen and Non-Knudsen Porous Materials," Int. J. Thermophys., **30**(4), pp. 1343–1356.
[28] Yasumoto, I., 1987, "Accommodation Coefficients of Helium, Neon, Argon, Hydrogen, and Deuterium on Graphitized Carbon," J. Phys. Chem., **91**(16), pp. 4298–4301.
[29] Hu, L., and McGaughey, A. J. H., 2013, "Energy Accommodation Between Noble Gases and Carbon Nanotubes," J. Phys. Chem. C, **117**(37), pp. 18804–18808.
[30] Amdur, I., and Guildner, L. A., 1957, "Thermal Accommodation Coefficients on Gas-Covered Tungsten, Nickel and Platinum," J. Am. Chem. Soc., **79**(2), pp. 311–315.
[31] Rader, D. J., Grasser, T. W., Castaneda, J. N., Trott, W. M., and Torczynski, J. R., 2005, "Measurements of Thermal Accommodation Coefficients," U.S. Department of Energy, Springfield, VA, Report No. SAND2005-6084.
[32] Fletcher, L., and White, F., 1984, *Heat Transfer and Fluid Flow Data Books*, Genium Publishing, Schnectady, NY.
[33] Fricke, H., 1924, "A Mathematical Treatment of the Electric Conductivity and Capacity of Disperse Systems—I: The Electric Conductivity of a Suspension of Homogeneous Spheroids," Phys. Rev., **24**(5), pp. 575–587.
[34] Stark, C., and Fricke, J., 1993, "Improved Heat-Transfer Models for Fibrous Insulations," Int. J. Heat Mass Transfer, **36**(3), pp. 617–625.
[35] Evans, W. J., Shen, M., and Keblinski, P., 2012, "Inter-Tube Thermal Conductance in Carbon Nanotubes Arrays and Bundles: Effects of Contact Area and Pressure," Appl. Phys. Lett., **100**(26), p. 261908.
[36] Yang, J., Waltermire, S., Chen, Y., Zinn, A. A., Xu, T. T., and Li, D., 2010, "Contact Thermal Resistance Between Individual Multiwall Carbon Nanotubes," Appl. Phys. Lett., **96**(2), p. 023109.